electronics

MDPI

Article

Research on the Inhibition and Transmission Properties of Photonic Spiking Dynamics in Semiconductor Ring Lasers

Xueting Zhang, Penghua Mu *, Guopeng Liu, Yiqiao Wang and Xueyuan Li *

School of Physics and Electronic Information, Yantai University, Yantai 264005, China; zhangxueting315@s.ytu.edu.cn (X.Z.); liuguopeng@s.ytu.edu.cn (G.L.); wangyiqiao@s.ytu.edu.cn (Y.W.)
* Correspondence: ph_mu@ytu.edu.cn (P.M.); lixueyuan@ytu.edu.cn (X.L.)

Abstract: Significant progress has been made in the research of all-optical neural networks in recent years. In this paper, we theoretically explore the properties of a neural system composed of semiconductor ring lasers (SRLs). Our study demonstrates that external optical signals generated by a tunable laser (TL) are injected into the first semiconductor ring laser photonic neuron (SRL1). Subsequently, the responses of SRL1 in the clockwise (CW) and counterclockwise (CCW) directions are unidirectionally injected into the CW and CCW directions of the second semiconductor ring laser photonic neuron (SRL2), respectively, which then exhibits similar spiking inhibition behaviors. Numerical simulations reveal that the spiking inhibition behavior of the SRL response can be precisely controlled by adjusting the perturbation time and intensity of the external injection signal, and this behavior is highly repeatable. Most importantly, we successfully achieve the stable transmission of these responses between the two SRL photonic neurons. These inhibition behaviors are analogous to those of biological neurons, but with a response speed reaching the sub-nanosecond level. Additionally, we indicate that SRL photonic neurons undergo a refractory-period-like phenomenon when subjected to two consecutive perturbations. These findings highlight the immense potential for the design and implementation of future all-optical neural networks, providing critical theoretical foundations and support for them.

Keywords: semiconductor ring laser; photonic neuron; spiking dynamics; inhibition

Citation: Zhang, X.; Mu, P.; Liu, G.; Wang, Y.; Li, X. Research on the Inhibition and Transmission Properties of Photonic Spiking Dynamics in Semiconductor Ring Lasers. *Electronics* **2024**, *13*, 2918. https://doi.org/10.3390/electronics13152918

Academic Editor: Nakkeeran Kaliyaperumal

Received: 1 July 2024
Revised: 20 July 2024
Accepted: 23 July 2024
Published: 24 July 2024

1. Introduction

It is well known that with the advent of the big data era, the volume of data has grown significantly. However, computers developed based on Moore's law are facing memory walls and power consumption bottlenecks, making it increasingly difficult to meet the massive data processing demand. In contrast, the human brain demonstrates superior performance in computation, capable of simultaneously processing multiple signals with an extremely low level of power consumption. Although pulsed neural networks based on microelectronics have made significant advancements in information processing technology, they are still limited in terms of energy consumption and speed. Optical platforms, with their unique advantages of a high speed, wide bandwidth, and low level of power consumption, show tremendous potential in the field of information processing.

In recent years, photonic systems have garnered significant attention from researchers due to their potential in the study and simulation of neuromimetic phenomena [1], especially in photonic recurrent neural networks [2] and photonic reservoir computing systems [3,4], which have achieved remarkable progress. Concurrently, a large number of scholars have discovered that photonic systems can also be used to simulate the spiking dynamic behavior of neurons [5,6], thus advancing the in-depth study of excitable systems [7]. Among these, optical injection systems are particularly remarkable due to their sufficiently nonlinear properties, which can generate excitable behavior and are well suited for both

experimental and theoretical analyses. More importantly, the pulse sequences generated by these systems have periods and pulse lengths several orders of magnitude shorter than those of biological neurons and exhibit excellent deterministic control capabilities. Under such configurations, excitable responses have been observed in various types of devices, including vertical-cavity surface-emitting lasers (VCSELs) [8,9], quantum dot (QD) devices [10–12], and semiconductor ring lasers (SRLs) [13]. For example, B. Kelleher's research team in Ireland conducted in-depth studies on optical injection in single-mode QD lasers and found that excitability pulse phenomena can occur under injection-locked boundary conditions. They also systematically analyzed the phase characteristics of these excitability pulses [12]. Subsequently, the team led by A. Hurtado in the UK investigated neuron-like properties based on VCSELs, initially studying the excitatory responses of an individual VCSEL under external stimulation. They then introduced an additional VCSEL photonic neuron and studied the communication properties between the two VCSEL neurons. These VCSEL-based neurons exhibit threshold characteristics in response to external stimulation intensity [8,14]. In 2011, photonic neurons based on SRL were studied by scientists including W. Coomans from Belgium, with SRLs triggered by external light to generate pulses, revealing a mechanism by which multiple consecutive excitatory pulses are triggered by a stimulus [15]. It is very noteworthy that the team led by Shuiying Xiang at Xi'an University of Electronic Science and Technology in China similarly conducted extensive research on VCSEL photonic neurons [9,16–20]. Moreover, in the past two years, they proposed and fabricated for the first time an integrated Fabry–Pérot laser pulse chip based on saturable absorbers (FP-SAs), experimentally validating its dynamic neuronal properties [21]. Similarly, this team also successfully fabricated and demonstrated a photonic synapse chip based on distributed feedback lasers with saturable absorbers (DFB-SAs), capable of simultaneously achieving linear weighting and non-linear spike activation functions [22]. These research achievements provide crucial support for the development of photonic neural networks. Recently, our research group investigated the excitatory spiking properties of optical injection into a single SRL system and successfully achieved various discharge forms of neurons, including phase spikes, rebound spikes, sustained spike discharges, and subthreshold oscillations [13].

Despite important advancements in the study of excitatory responses, it is equally critical to recognize the pivotal role of inhibitory neurons in regulating brain-like functions. The intricate functionality of inhibitory neurons within neural circuitry has been well established by extensive research [15,23]. In biological neural networks, inhibitory neurons achieve suppression through intermediate neurons within local neural circuits, a process crucial for shaping neural discharge patterns and balancing network excitability. Furthermore, inhibition not only holds significance in neural computation but also provides causal information about neuronal subgroups, which aids in deeper investigations into their behavioral impacts [24]. Additionally, in biological neurons, there exist dynamic properties such as refractory periods, which limit the propagation speed of action potentials and thus influence the information transmission rates in neural networks. For instance, the human ear cannot distinguish sound frequencies beyond a certain threshold. Therefore, research on inhibitory neurons holds vital value in understanding and simulating complex brain-like functions. In this regard, numerous scholars have embarked on related studies. For example, the team led by A. Hurtado explored threshold properties, encoding properties, and inhibition features of VCSEL photonic neurons based on the transition mechanisms between injection-locked and pulsing states in single and dual VCSEL configurations [14,25,26]. In 2013, a team from Princeton University studied leaky integrate and fire (LIF) neuron models and simulated integral, threshold, and post-emission refractory period characteristics using a VCSEL with built-in saturable absorbers (VCSEL-SAs) [27]. In 2018, a team from Southwest University in China investigated the transmission properties of inhibitory spiking signals between two unidirectionally coupled VCSELs [28], making important contributions to future photonic neural networks.

However, experimental studies on the inhibitory properties of photonic neurons based on optical injection in SRLs have not yet been conducted so far. The active cavity of an SRL features a unique circular geometry capable of generating light outputs in two directions, i.e., clockwise (CW) and counterclockwise (CCW) modes. This characteristic endows SRLs with high levels of integration and scalability, making them highly promising for achieving fully integrated photonic neural networks and all-optical devices. Therefore, it is of great importance to investigate the spike suppression signal transmission properties of optically injected SRL neural systems.

In this paper, we demonstrate the generation of inhibitory spiking signals in two unidirectionally coupled SRL neural systems, along with their transmission properties and the effects of injecting two consecutive pulses with perturbations. Specifically, the first photonic neuron, SRL1, is perturbed by external injected light, and its output is injected into the second photonic neuron, SRL2. The organization of this paper is structured as follows. In Section 2, the models of the two unidirectionally coupled SRL systems and their corresponding rate equations are presented in detail. Section 3 analyzes the effects of externally injected light perturbation time and intensity on the inhibitory responses and transmission properties of SRL1 and SRL2 outputs in depth. Subsequently, we further investigate the output properties of the system for two successive external perturbation injections. In the end, in Section 4, the main conclusions of this study are summarized.

2. Theory and Models

The schematic diagram in Figure 1 illustrates the structure of two unidirectionally coupled SRL photonic neurons. This system consists of two SRLs, namely, the first photonic neuron, SRL1, and the second photonic neuron, SRL2. The input section of the system consists of a tunable laser (TL), a signal generator (SG), and a modulator (Mod), which generates an external injection signal. This signal is split into two parts after passing through a polarization controller (PC) and a 50:50 fiber coupler (FC). Among these, 50% of the light is directed through a variable optical attenuator (VA1) and injected into the CW mode of SRL1, and its output signal, after passing through VA3, is injected into the CW mode of SRL2 (as indicated by the black paths in the latter half of Figure 1). Similarly, the remaining 50% of the light passes through VA2 and is injected into SRL1's CCW mode, and its output is injected into SRL2's corresponding CCW mode (as indicated by the red paths in the latter half of Figure 1) after passing through VA4. Note that the injection intensity can be easily adjusted by the VAs to achieve precise control of the system. The rate equations of the proposed SRL neural system are as follows [29–32]:

$$\frac{dE_1^{CW/CCW}}{dt} = \kappa(1+i\alpha)[g_1N_1-1]E_1^{CW/CCW} - k(1\mp\delta_k)e^{i\phi}E_1^{CCW/CW} + k_{inj1/2}E_{inj}e^{i2\pi\Delta f_{1/2}t} \tag{1}$$

$$\begin{aligned}\frac{dE_2^{CW/CCW}}{dt} &= \kappa(1+i\alpha)[g_2N_2-1]E_2^{CW/CCW} - k(1\mp\delta_k)e^{i\phi}E_2^{CCW/CW} \\ &+k_{inj3/4}E_1^{CW/CCW}\left(t-\tau_{inj}\right)e^{(-i\omega\tau_{inj}-i2\pi\Delta f_{3/4}t)}\end{aligned} \tag{2}$$

$$\begin{aligned}\frac{dN_i^{CW/CCW}}{dt} &= \gamma[\mu - N_i^{CW/CCW} - g_i^{CW/CCW}N_i^{CW/CCW}|\ E_i^{CW/CCW}\ |^2 \\ &-g_i^{CCW/CW}N_i^{CW/CCW}|\ E_i^{CCW/CW}\ |^2]\end{aligned} \tag{3}$$

$$g_i^{CW/CCW} = 1 - s|\ E_i^{CW/CCW}\ |^2 - c|\ E_i^{CCW/CW}\ |^2 \tag{4}$$

where $E(t)$ represents the complex electric field amplitude, $N(t)$ denotes the carrier density, and $g(t)$ indicates the gain. The subscripts 1 and 2 correspond to SRL1 and SRL2, respectively, with subscript i taking values of 1 and 2. κ is the electric field decay rate, α is the linewidth enhancement factor, k is the backscattering rate, δ_k is the asymmetry factor, ϕ is the phase shift, γ is the carrier decay rate, μ is the renormalized injection current, s is the self-saturation coefficient, and c is the cross-saturation coefficient. The last terms in

Equations (1) and (2) denote injection components, where Equation (1) signifies the injection from TL, and Equation (2) stands for the injection from SRL1. In the injection terms, k_{inj1} and k_{inj2} represent the injection intensities from TL in the CW and CCW directions, respectively, while k_{inj3} and k_{inj4} denote the injection intensities from the SRL1 outputs into SRL2. E_{inj} stands for the slowly varying electric field injected from TL in the CW and CCW directions. τ_{inj} signifies the injection delay time from SRL1 to SRL2. $\Delta f_{1/2}$ is the frequency detuning between TL and the CW/CCW of SRL1, $\Delta f_{3/4}$ is the frequency detuning between SRL1 and SRL2, and ω stands for the corresponding angular frequency of the SRL.

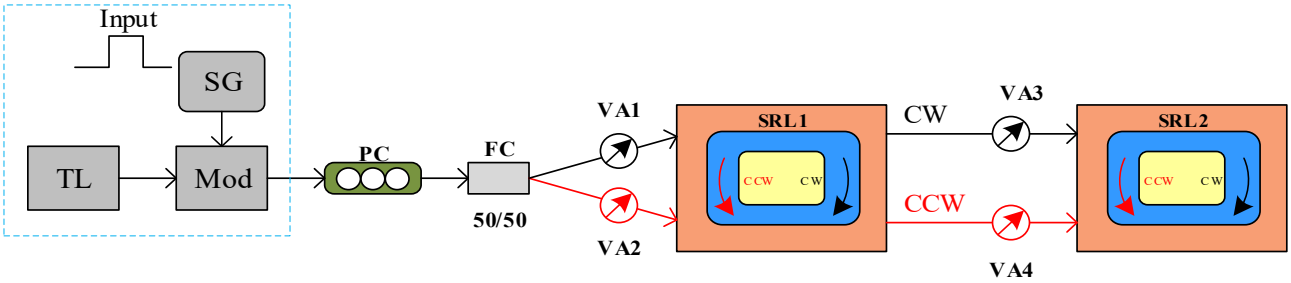

Figure 1. Schematic structure of unidirectionally coupled SRL photonic neurons. TL: tunable laser; Mod: modulator; SG: signal generator; PC: polarization controller; VA: variable optical attenuator; SRL1: the first semiconductor ring laser; SRL2: the second semiconductor ring laser; FC: fiber coupler.

Specifically, the key parameters of the two lasers are listed in Table 1, where the relevant definitions and specific values are given, and other system parameters will be detailed in the subsequent simulation section. In this study, we numerically solve the rate Equations (1)–(4) using the fourth-order Runge–Kutta method. It should be noted in particular that we analyze the output of the SRL in a fully symmetric state; i.e., the parameters across both modes of SRLs are identical. Moreover, the interference of noise and temperature is neglected in the simulation process.

Table 1. The parameters used in the simulation [13,30].

Parameter	Description	Value
κ	Field decay rate	100 ns^{-1}
α	Linewidth enhancement factor	3.3
k	Backscattering rate	0.44 ns^{-1}
δ_k	Asymmetry factor	0.2
ϕ	Phase shift	3
γ	Carrier decay rate	0.2 ns^{-1}
μ	Renormalized injection current	5
s	Self-saturation coefficient	0.005
c	Cross-saturation coefficient	0.01
τ_{inj}	Injection delay time	0.01 ns

3. Results and Discussion

The schematic of the device in Figure 1 shows a typical external input signal (dashed lines), whose characteristics are depicted in Figure 2. A typical injection signal features a constant injection level E_{inj}, a controllable perturbation strength K, and a perturbation time td. Here, the ratio of the perturbation intensity K to the constant injection level E_{inj} is defined as Kp; i.e., $Kp = K/E_{inj}$. By adjusting these parameters, the influence of the external signal on the system can be precisely controlled to study the dynamic responses of photonic neurons under different perturbation conditions.

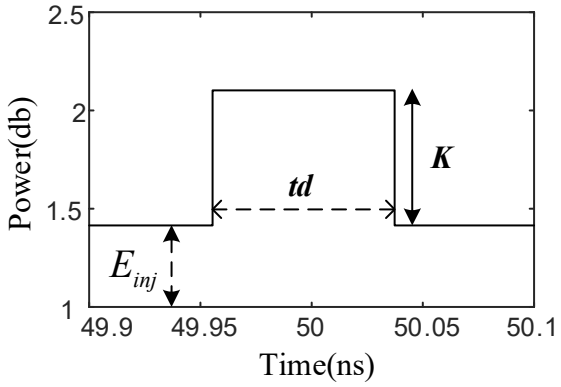

Figure 2. A typical external injection signal. E_{inj} is the constant injection level, K is the controllable perturbation strength, and td is the perturbation time.

Through theory and modeling, we design an external perturbation signal generated by the TL to demonstrate the complex neural-like dynamics of the photonic inhibition of spiking neurons. In this study, we first examine the response of SRL1 under external optical stimulation. To be more precise, the injection intensities k_{inj1} and k_{inj2} for the CW and CCW directions of SRL1 are both set equal to 10 ns^{-1}, and the detuning frequencies Δf_1 and Δf_2 between the TL and CW/CCW are both set to -3.7 GHz. The results are shown in Figure 3a. The black inset at the top of Figure 3a represents the external injection signal, where the constant injection level E_{inj} = 0.9, the duration td of the applied perturbation signals is 2.8 ns, and the intensity Kp = 1.15. To clearly illustrate the outputs, we plot both output signals of SRL1 on a single graph, where the CW output signal is vertically shifted upward by 5.5 units. From Figure 3a, it can be observed that under a constant injection level, i.e., in the absence of external stimulation, both the CW and CCW signals of SRL1 operate in a continuous tonic spiking state. When the external perturbation reaches 50 ns, the injection intensity suddenly increases, driving SRL1 into an injection-locked state, and the tonic spiking signal is suppressed. After the perturbation duration of 2.8 ns, the suppressed response disappears, and SRL1 switches back to the tonic spiking state. This phenomenon arises because the sudden increase in intensity places SRL1 at the boundary between the locked and unlocked states, which causes it to toggle back and forth between these states. This toggling is repetitive [33]. Furthermore, it is particularly important to note that we study a completely symmetric SRL; thus, the SRL has a bistable state. In other words, the SRL can exist in two stable distribution states simultaneously. However, the pulse intensity of the CCW output is significantly larger than that of the CW output, which is due to the fact that the ring laser in a bistable state exhibits unidirectional behavior under direct current modulation [34–37], a phenomenon that is also clearly observed in Figure 3.

In order to validate the effectiveness and stability of the inhibition response, we present the time maps of SRL1 under continuous perturbations, as shown in Figure 3(a1,a2). In these maps, the color transition from blue to yellow indicates the gradual increase in signal intensity, with the horizontal axis representing the cycle number and the vertical axis representing the time within the cycle. From Figure 3(a1,a2), it is evident that both the CW and CCW outputs of SRL1 can produce stable inhibition behavior for 100 continuous perturbations (no single straight-line regions are observed), which demonstrates the repeatability of this inhibition behavior.

Subsequently, the two output signals from SRL1 are unidirectionally injected into SRL2, whose response is shown in Figure 3b. Herein, the detuning frequencies Δf_3 and Δf_4 between SRL1 and SRL2 are set to -4 GHz, the injection intensities of the two lasers in the same directions are k_{inj3} (the CW direction) and k_{inj4} (the CCW direction), and $k_{inj3} = k_{inj4}$ = 85 ns^{-1}. As depicted in Figure 3b, under continuous injections from SRL1, the response of SRL2 transitions from a tonic spiking state to injection-locking and back

to tonic spiking, which indicates that SRL2 also exhibits inhibition behavior under the corresponding external perturbation. Obviously, both lasers show similar responses to external disturbances under the simulation conditions we set. The temporal maps corresponding to SRL2 are shown in Figure 3(b1,b2). The results clarify that SRL1 can achieve consistent and repeatable spiking inhibition under continuous external perturbations, and this behavior can be propagated in turn to SRL2, thereby demonstrating the communication of inhibitory neuron responses at sub-nanosecond speeds in the photonic neuron networks based on SRLs. This inhibition behavior exhibits significant similarity to biological neurons, which undergo transitions from normal firing to inhibition and back to normal firing in response to external stimuli. Such processes are crucial in neural networks as they facilitate information transmission and processing.

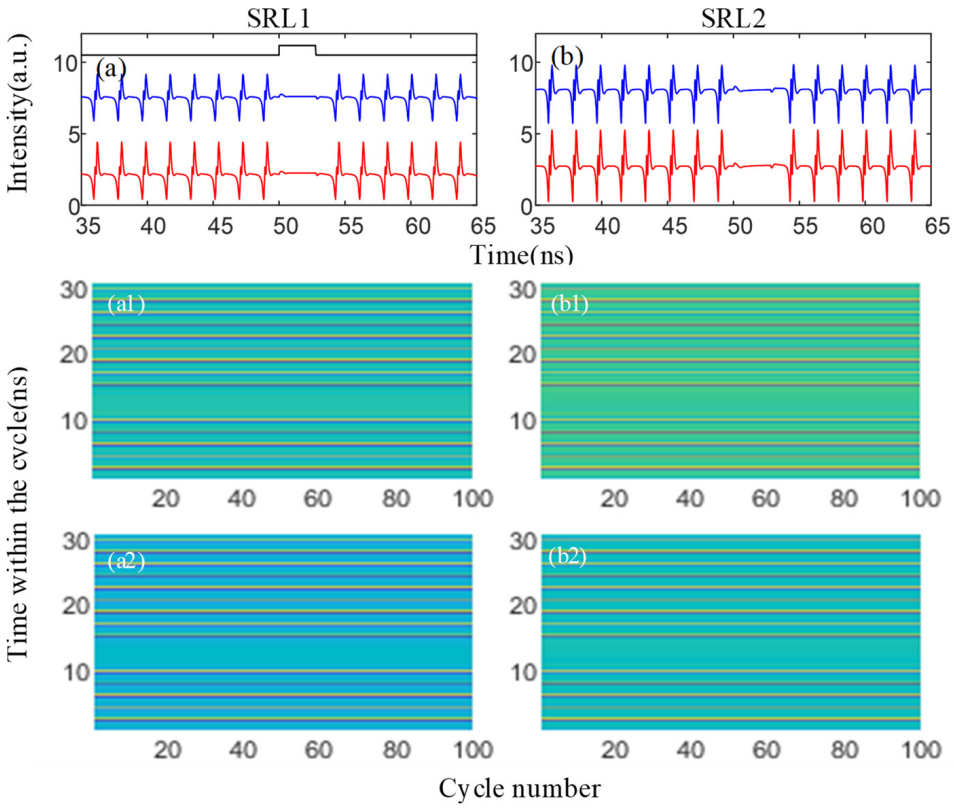

Figure 3. Time series plots (**a**,**b**) and temporal maps (**a1**,**b2**) of the outputs from SRL1 and SRL2. Blue denotes CW, and red denotes CCW. (**a**,**a1**,**a2**): SRL1; (**b**,**b1**,**b2**): SRL2. *td* = 2.8 ns and *Kp* = 1.15. The black inset in (**a**) represents the external injection signal.

To further explore the transmission properties of peak inhibition behavior between two interconnected SRL photonic neurons and the effect of external injection signals on their output responses, we numerically simulate the cases of SRL1 and SRL2 with external perturbation times *td* ranging from 1.5 ns to 5.2 ns. The time series outputs are shown in Figure 4, in which *Kp* is fixed at 1.15. As can be seen in Figure 4(a1), when there is no disturbance in the initial state, SRL1 exhibits continuous tonic spiking with sub-nanosecond intervals under successive external optical injections. Upon the perturbation reaching *td* = 1.5 ns, SRL1 is forced into an injection-locked state due to the perturbation time reaching the critical threshold. This state suppresses the tonic spiking activity of SRL1. After the perturbation time ends, SRL1 returns to an unlocked state and resumes tonic spiking. This indicates that the tonic spiking signals in both the CW and CCW directions at the output of SRL1 are suppressed throughout the disturbance window. Then, as the perturbation time gradually increases to 2.8 ns (Figure 4(a2)), 4 ns (Figure 4(a3)), and 5.2 ns (Figure 4(a4)), the tonic spiking of SRL1 is completely suppressed during the respective disturbance periods,

meaning that the suppression range of tonic spikes increases with the extension of the perturbation time. This phenomenon occurs because SRL1 is forced from a spiking state into an injection-locked state. As the perturbation time is extended, the system remains in the injection-locked state for a longer duration, thereby more effectively suppressing the tonic spikes. It is clear that the window of inhibitory spiking dynamics can be controlled by adjusting *td*. Next, when the output dynamics of SRL1 are transmitted and integrated into SRL2, SRL2 can obtain similar responses, as vividly depicted in Figure 4(b1–b4). This suggests that different and controllable lengths of inhibitory spiking dynamics from SRL1 can be successfully transmitted to SRL2, thus enabling effective communication between the two interconnected SRLs. This behavior again parallels that observed in biological neuron systems, but they operate at speeds approximately eight orders of magnitude faster.

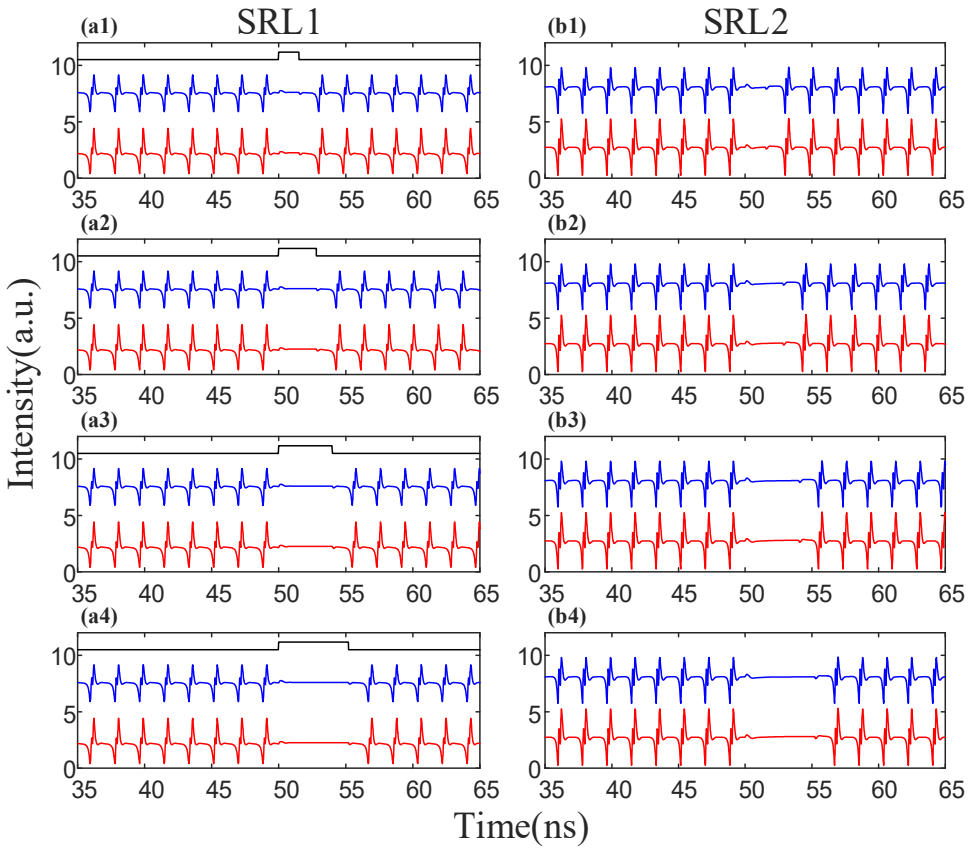

Figure 4. Time series plots of SRL1 (**a1**–**a4**) and SRL2 (**b1**–**b4**) outputs under different *td* values. Blue represents CW, and red represents CCW. (**a1**,**b1**): *td* = 1.5 ns, (**a2**,**b2**): *td* = 2.8 ns, (**a3**,**b3**): *td* = 4 ns, and (**a4**,**b4**): *td* = 5.2 ns. Here, *Kp* = 1.15.

Furthermore, Figure 5 sequentially presents the response time maps of SRL1 and SRL2 in both the CW and CCW directions. Each map in Figure 5 consists of nine time periods, with 20 consecutive event perturbations plotted within each period, where *td* varies progressively from 1.5 ns to 10.7 ns. The other parameters remain consistent with those in Figure 4, and the perturbation intensity color coding is the same as described above. It is evident from Figure 5 that by adjusting the perturbation time *td* of SRL1, we are able to obtain a controlled and repeatable dynamic spiking inhibition pattern. This controllability indicates that SRL1 effectively suppresses tonic spiking throughout the duration of external disturbances by accurately entering and exiting the injection-locked states at different perturbation times. In addition, the dynamic state output of SRL1 is successfully transferred to SRL2 via a unidirectional injection, causing SRL2 to exhibit similar spiking inhibition behavior under identical perturbation conditions. This further confirms the stable transmission of spiking inhibition dynamics between SRL1 and SRL2.

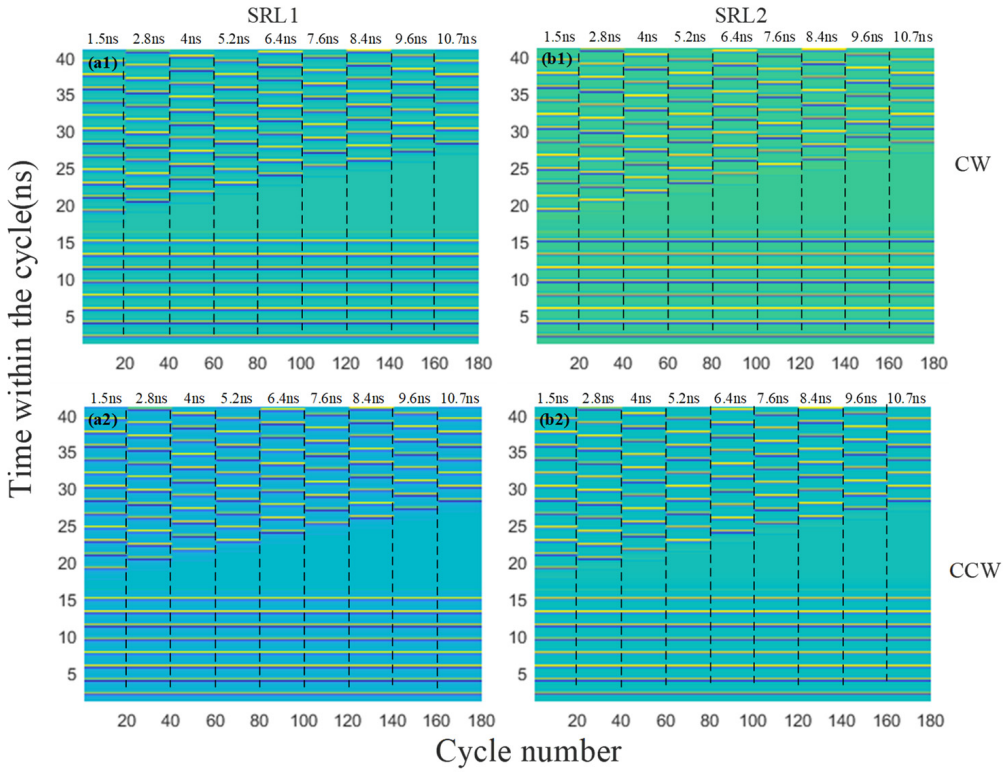

Figure 5. Time maps of SRL1 (**a1**,**a2**) and SRL2 (**b1**,**b2**) outputs under different *td* values. The first row represents CW, and the second row represents CCW. The plots combine different *td* values ranging from 1.5 ns to 10.7 ns. Here, $Kp = 1.15$.

The threshold intensity response characteristic is a key feature in neuron models. To delve into its impact on the inhibitory response of SRL1 photonic neurons, we examine how variations in the external perturbation intensity *Kp* affect the system outputs. Figure 6 illustrates the time series plots of SRL1 and SRL2 outputs in the CW and CCW directions under external perturbation intensities ranging from $Kp = 0.84$ to $Kp = 1.2$, and the perturbation duration $td = 6.4$ ns. In the following simulations, we adjust the detuning frequency between SRL1 and SRL2 to $\Delta f_3 = \Delta f_4 = -4.5$ GHz, and the rest of the parameters are kept constant. For the case of $Kp = 0.84$, the response of SRL1 excites irregular oscillatory spiking signals throughout the perturbation window as seen in Figure 6(a1). As the perturbation intensity *Kp* is increased to 0.89 and 0.98, it is observed that from Figure 6(a2,a3), spiking signals still occur within the perturbation duration, but their amplitude and frequency change. This result shows that with relatively low perturbation intensities, the number of spiking signals during the perturbation interval decreases. However, the situation changes significantly as the perturbation intensity further increases. From Figure 6(a4), it can be seen that for the case in which the value of *Kp* is 1.2, the tonic spiking signals are completely suppressed during the perturbation period. This suppression occurs because when the perturbation intensity reaches a certain threshold level, tonic spiking signals are completely inhibited as long as perturbations are present. Physically, this can be explained as when the injection intensity of perturbations increases to a sufficiently high level, it is enough to force SRL1 into an injection-locked state, which results in the complete inhibition of the tonic spiking signals within the perturbation interval. On the other hand, these inhibitory dynamic behaviors of SRL1 can be successfully transferred to SRL2, which shows a similar response pattern to that of SRL1, as shown in Figure 6(b1–b4). This indicates that the perturbation intensity of the second photonic neuron must also reach a certain threshold level in order to achieve spike suppression. This phenomenon demonstrates that external perturbations need to exceed a critical intensity threshold to suppress tonic spiking signals in SRL1. Moreover, by regulating the perturbation intensity, the stable transmission of

spiking inhibition behaviors can be achieved in interconnected SRL systems. Similarly, in biological neural networks, neurons stop firing pulses only when the intensity of an external stimulus exceeds a certain threshold. This behavior is also reproduced in our photonic neuron system described above, further validating its effectiveness and reliability as a neuron-like model.

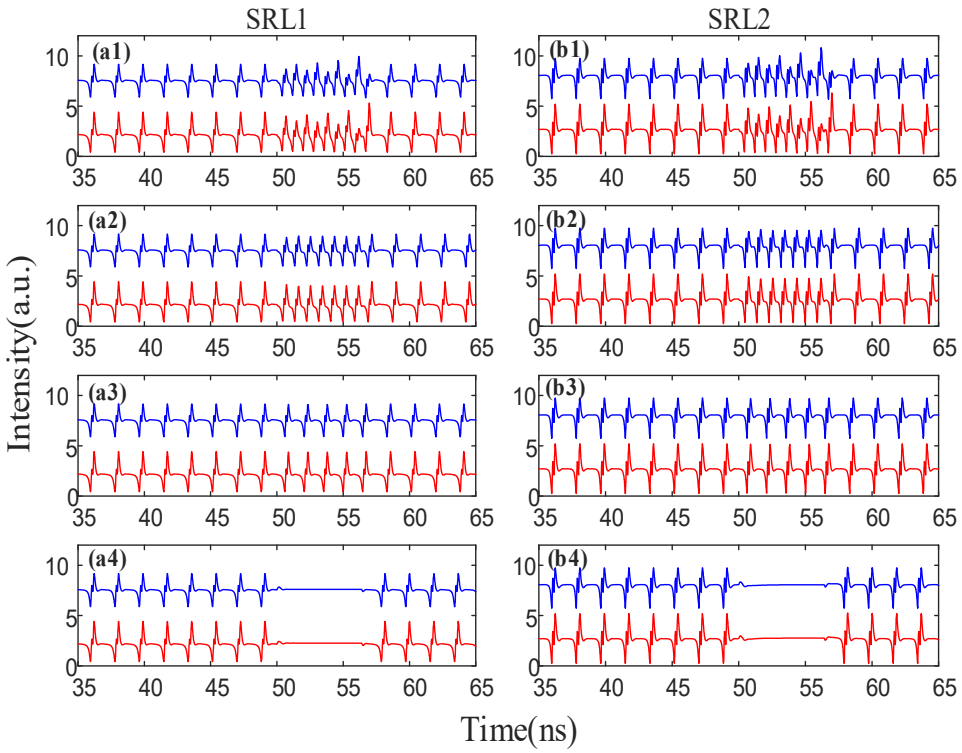

Figure 6. Time series plots of SRL1 (**a1**–**a4**) and SRL2 (**b1**–**b4**) outputs under different *Kp* values. Blue represents CW, and red represents CCW. (**a1**,**b1**): *Kp* = 0.84, (**a2**,**b2**): *Kp* = 0.89, (**a3**,**b3**): *Kp* = 0.98, and (**a4**,**b4**): *Kp* = 1.2. Here, *td* = 6.4 ns.

Furthermore, the corresponding time maps for Figure 6(a1–a4),(b1–b4) are given in Figure 7, illustrating the response behavior of SRL1 and SRL2 to 20 consecutive perturbations at four different *Kp* values. As depicted in Figure 7, at perturbation intensities of *Kp* = 0.84, 0.89, and 0.98, both SRL1 and SRL2 display distinct spiking signals consistently throughout the entire duration of the simulation period. However, there are obvious differences in the number and amplitude of the spiking signals, which suggests that different perturbation intensities affect the properties of the spiking signals. When *Kp* reaches 1.2, surpassing the critical threshold of the perturbation intensity, the system experiences a complete suppression of spiking signals, indicating a robust response to higher external stimuli. This result further corroborates the conclusions drawn from Figure 6. It is clear that by varying the perturbation intensity, the spiking inhibition dynamics of SRL1 can be easily controlled. More importantly, this peak spiking inhibition behavior of SRL1 can be effectively propagated to SRL2 in a stable manner, with both yielding analogous outcomes between the two lasers. Therefore, the responses of SRL1 and SRL2 to external perturbations not only show a high degree of consistency but also demonstrate controllability and repeatability. This phenomenon is comprehensively displayed in Figure 7.

It is well known that the refractory period is a fundamental component of excitatory neuronal activity [38]. Following a neuron's response to a stimulus, there is a subsequent period during which the neuron either does not respond or has a diminished response to further stimuli; this period is typically referred to as the refractory period. This concept is generally divided into two phases: the absolute refractory period and the relative refractory period. This means that during the absolute refractory period, the neuron is entirely

incapable of generating a new action potential. In the relative refractory period, although it is more challenging to trigger an action potential, it is still possible with sufficiently strong stimuli. In addition, the refractory period of excitable systems can be considered critical for excitability logic and pulse shaping, in which the speed of information processing is also dependent on this parameter. On the other hand, inhibitory neurons play a regulatory and constraining role in neural networks, and their activity patterns have profound impacts on the overall function of the neural network. Therefore, whether inhibitory neurons possess a similar refractory period is an intriguing question worthy of investigation.

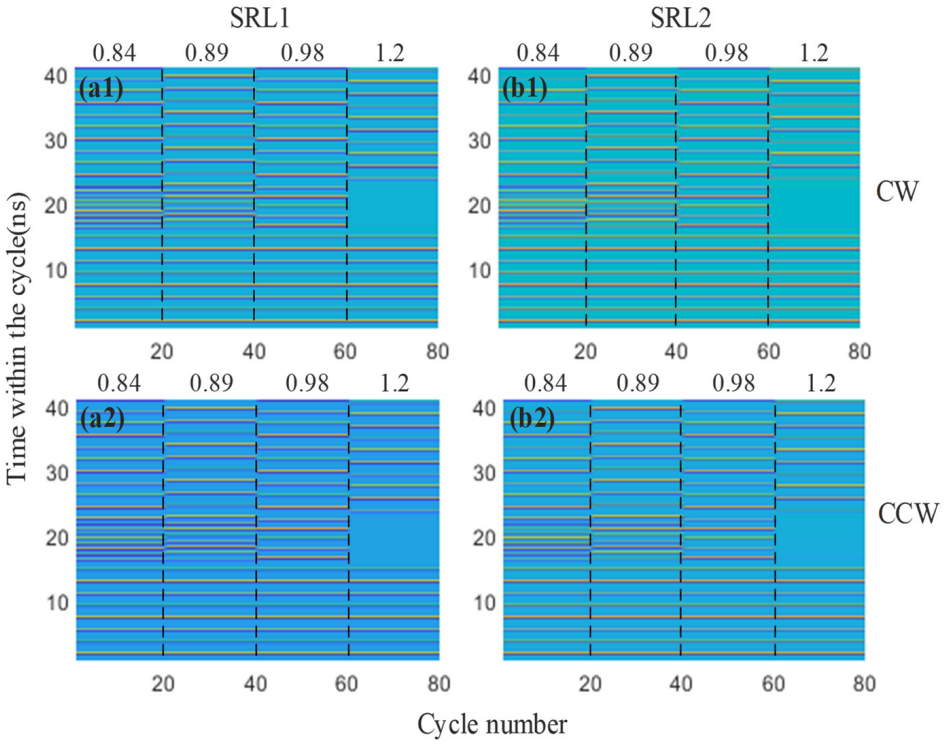

Figure 7. Time maps of SRL1 (**a1**,**a2**) and SRL2 (**b1**,**b2**) outputs under different *Kp* values. The first row represents CW, and the second row represents CCW. The plots combine different *Kp* values (0.84, 0.89, 0.98, and 1.2). Here, *td* = 6.4 ns.

To investigate the refractory-like properties of SRLs, we introduce two consecutive external perturbations in the externally injected signals into the SRL neural system. In this following study, we define a new parameter: the time interval between perturbations (*tin*). Both perturbation durations, td_1 and td_2, are set to 4 ns, and the perturbation intensities, Kp_1 and Kp_2, are identical, both at 1.2. The other system parameters are set as follows: $k_{inj1} = k_{inj2} = 10\ \text{ns}^{-1}$, $\Delta f_3 = \Delta f_4 = -4.5$ GHz, $k_{inj3} = k_{inj4} = 85\ \text{ns}^{-1}$, $\Delta f_3 = \Delta f_4 = -4.5$ GHz, and the remaining parameters are the same as in the previous simulations. Figure 8 shows the time series plots of the outputs of SRL1 and SRL2 at different perturbation time intervals (*tin*); the time interval between the two perturbation signals is not easily discernible when the *tin* is small, so a small inset is added in Figure 8(a2) to clearly show this time interval. It can be seen that from Figure 8(a1), when the *tin* = 10 ns, SRL1 achieves spiking inhibition within the two perturbation periods td_1 and td_2, respectively, while generating tonic spikes in the 10 ns interval between the two perturbations. This indicates that a sufficiently long perturbation interval allows SRL1 to achieve inhibition within both perturbation periods. In contrast, when the *tin* between the two perturbations is very short, only 0.001 ns, SRL1 generates only one inhibitory response within the two perturbation periods, as shown in Figure 8(a2). This phenomenon arises because the second perturbation signal arrives with an insufficient inter-stimulus interval, thereby impeding the carriers' recovery to the inhibition threshold. Consequently, this rapid succession hinders the laser's ability

to adequately respond to the subsequent perturbation signal, highlighting the impact of timing intervals on the system's responsiveness. Moreover, this phenomenon bears a remarkable resemblance to the refractory period. To gain a deeper understanding of the transmission characteristics of this dynamic state, see Figure 8(b1,b2). It can be observed in Figure 8(b1) that when the *tin* = 10 ns, SRL2 achieves spike suppression during the two perturbation periods td_1 and td_2, while still generating tonic spikes outside these periods, similar to the output of SRL1. Similarly, when the *tin* = 0.001 ns, the response of SRL2 remains analogous to that of SRL1, with SRL2 producing only one inhibitory response during the two perturbation periods and failing to generate tonic spikes in the *tin*. These results further verify that the output of SRL1 under two successive perturbation signals can also be effectively transmitted to SRL2 and produce similar responses. This further validates the results of Figures 4 and 6.

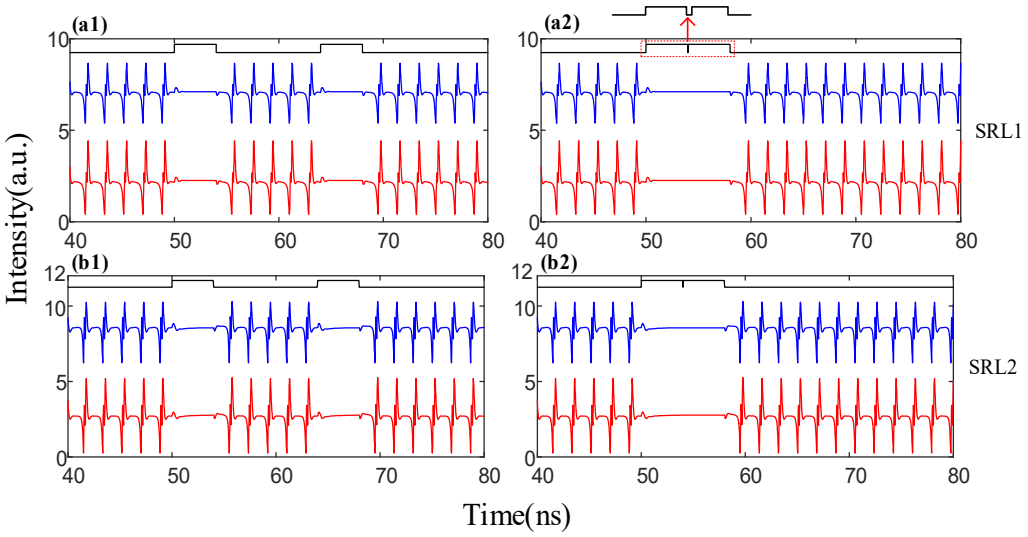

Figure 8. Time series plots of SRL1 and SRL2 outputs at different perturbation intervals (*tin*). The first row represents the output of SRL1, and the second row represents the output of SRL2. CW is depicted in blue, and CCW is shown in red. (**a1**,**b1**): *tin* = 10 ns; (**a2**,**b2**): *tin* = 0.001 ns. Here, $td_1 = td_2 = 4$ ns, and $Kp_1 = Kp_2 = 1.2$.

4. Conclusions

In summary, we conducted a numerical study based on the rate equations of two unidirectionally coupled SRL photonic neural systems in detail and successfully demonstrate the communication of the inhibitory tonic spiking dynamics mechanism within this system. In particular, the external injection signal generated by the TL is injected into the first photonic neuron SRL1. By precisely adjusting the external perturbation time and intensity, we are able to effectively control the spiking inhibition behavior of SRL1. Subsequently, the outputs of SRL1 in the CW and CCW directions are unidirectionally injected into the CW and CCW directions of the second photonic neuron, SRL2, respectively, and SRL2 exhibits similar spiking inhibition responses to those of SRL1. Our findings reveal that the spiking inhibition behavior induced in the SRL photonic neuron model by external stimuli is analogous to that observed in inhibitory biological neurons in the brain, but with a much faster response speed reaching the sub-nanosecond level. More importantly, we succeeded in achieving the stable transmission of spiking inhibition dynamics between two SRL photonic neurons. Furthermore, we also demonstrate that under the condition of two consecutive perturbations, SRL photonic neurons exhibit a phenomenon similar to the "refractory period." These results provide robust theoretical support for the future establishment of neural models and networks.

Author Contributions: Methodology, X.Z. and P.M.; validation, G.L. and X.L.; investigation, X.L. and Y.W.; writing—original draft preparation, X.Z., P.M. and X.L.; writing—review and editing, X.Z., P.M., G.L., Y.W. and X.L. All authors have read and agreed to the published version of the manuscript.

Funding: This work was supported by the Natural Science Foundation of Shandong Provincial (ZR2020QF090), The Key Lab of Modern Optical Technologies of Education Ministry of China, Soochow University (KJS2066), and The Key Lab of Advanced Optical Manufacturing Technologies of Jiangsu Province, Soochow University (KJS2045).

Institutional Review Board Statement: Not applicable.

Informed Consent Statement: Not applicable.

Data Availability Statement: Data are contained within the article.

Acknowledgments: The authors would like to thank all the reviewers for their helpful comments and suggestions for this paper.

Conflicts of Interest: The authors declare no conflicts of interest.

References

1. *Neuromorphic Photonics*; Prucnal, P.R.; Shastri, B.J. (Eds.) CRC Press: Boca Raton, FL, USA, 2017; ISBN 978-1-315-37059-0.
2. Tait, A.N.; de Lima, T.F.; Zhou, E.; Wu, A.X.; Nahmias, M.A.; Shastri, B.J.; Prucnal, P.R. Neuromorphic Photonic Networks Using Silicon Photonic Weight Banks. *Sci. Rep.* **2017**, *7*, 7430. [CrossRef] [PubMed]
3. Photonic Reservoir Computing. Available online: https://www.degruyter.com/document/doi/10.1515/9783110583496/pdf?licenseType=restricted (accessed on 1 July 2024).
4. Moughames, J.; Porte, X.; Thiel, M.; Ulliac, G.; Larger, L.; Jacquot, M.; Kadic, M.; Brunner, D. Three-Dimensional Waveguide Interconnects for Scalable Integration of Photonic Neural Networks. *Optica* **2020**, *7*, 640–646. [CrossRef]
5. Lindner, B.; García-Ojalvo, J.; Neiman, A.; Schimansky-Geier, L. Effects of Noise in Excitable Systems. *Phys. Rep.* **2004**, *392*, 321–424. [CrossRef]
6. Izhikevich, E.M. Neural Excitability, Spiking and Bursting. *Int. J. Bifurcation Chaos* **2000**, *10*, 1171–1266. [CrossRef]
7. Prucnal, P.R.; Shastri, B.J.; de Lima, T.F.; Nahmias, M.A.; Tait, A.N. Recent Progress in Semiconductor Excitable Lasers for Photonic Spike Processing. *Adv. Opt. Photon. AOP* **2016**, *8*, 228–299. [CrossRef]
8. Deng, T.; Robertson, J.; Hurtado, A. Controlled Propagation of Spiking Dynamics in Vertical-Cavity Surface-Emitting Lasers: Towards Neuromorphic Photonic Networks. *IEEE J. Sel. Top. Quantum Electron.* **2017**, *23*, 1800408. [CrossRef]
9. Xiang, S.Y.; Zhang, H.; Guo, X.X.; Li, J.F.; Wen, A.J.; Pan, W.; Hao, Y. Cascadable Neuron-Like Spiking Dynamics in Coupled VCSELs Subject to Orthogonally Polarized Optical Pulse Injection. *IEEE J. Sel. Top. Quantum Electron.* **2017**, *23*, 1700207. [CrossRef]
10. Kelleher, B.; Bonatto, C.; Huyet, G.; Hegarty, S.P. Excitability in Optically Injected Semiconductor Lasers: Contrasting Quantum-Well- and Quantum-Dot-Based Devices. *Phys. Rev. E* **2011**, *83*, 026207. [CrossRef]
11. Goulding, D.; Hegarty, S.P.; Rasskazov, O.; Melnik, S.; Hartnett, M.; Greene, G.; McInerney, J.G.; Rachinskii, D.; Huyet, G. Excitability in a Quantum Dot Semiconductor Laser with Optical Injection. *Phys. Rev. Lett.* **2007**, *98*, 153903. [CrossRef]
12. Kelleher, B.; Goulding, D.; Hegarty, S.P.; Huyet, G.; Cong, D.-Y.; Martinez, A.; Lemaître, A.; Ramdane, A.; Fischer, M.; Gerschütz, F.; et al. Excitable Phase Slips in an Injection-Locked Single-Mode Quantum-Dot Laser. *Opt. Lett.* **2009**, *34*, 440–442. [CrossRef]
13. Mu, P.; Wang, K.; Liu, G.; Wang, Y.; Liu, X.; Guo, G.; Hu, G. Spike Dynamics Analysis in Semiconductor Ring Laser. *Electronics* **2024**, *13*, 260. [CrossRef]
14. Robertson, J.; Wade, E.; Kopp, Y.; Bueno, J.; Hurtado, A. Toward Neuromorphic Photonic Networks of Ultrafast Spiking Laser Neurons. *IEEE J. Sel. Top. Quantum Electron.* **2020**, *26*, 7700715. [CrossRef]
15. Coomans, W.; Gelens, L.; Beri, S.; Danckaert, J.; Van der Sande, G. Solitary and Coupled Semiconductor Ring Lasers as Optical Spiking Neurons. *Phys. Rev. E* **2011**, *84*, 036209. [CrossRef] [PubMed]
16. Xiang, S.; Wen, A.; Pan, W. Emulation of Spiking Response and Spiking Frequency Property in VCSEL-Based Photonic Neuron. *IEEE Photonics J.* **2016**, *8*, 1504109. [CrossRef]
17. Xiang, S.; Zhang, Y.; Guo, X.; Wen, A.; Hao, Y. Photonic Generation of Neuron-Like Dynamics Using VCSELs Subject to Double Polarized Optical Injection. *J. Light. Technol.* **2018**, *36*, 4227–4234. [CrossRef]
18. Zhang, Y.; Xiang, S.; Gong, J.; Guo, X.; Wen, A.; Hao, Y. Spike Encoding and Storage Properties in Mutually Coupled Vertical-Cavity Surface-Emitting Lasers Subject to Optical Pulse Injection. *Appl. Opt.* **2018**, *57*, 1731–1737. [CrossRef]
19. Xiang, S.; Gong, J.; Zhang, Y.; Guo, X.; Han, Y.; Wen, A.; Hao, Y. Numerical Implementation of Wavelength-Dependent Photonic Spike Timing Dependent Plasticity Based on VCSOA. *IEEE J. Quantum Electron.* **2018**, *54*, 8100107. [CrossRef]
20. Zhang, Y.; Xiang, S.; Guo, X.; Wen, A.; Hao, Y. Polarization-Resolved and Polarization- Multiplexed Spike Encoding Properties in Photonic Neuron Based on VCSEL-SA. *Sci. Rep.* **2018**, *8*, 16095. [CrossRef] [PubMed]

21. Xiang, S.; Shi, Y.; Guo, X.; Zhang, Y.; Wang, H.; Zheng, D.; Song, Z.; Han, Y.; Gao, S.; Zhao, S.; et al. Hardware-Algorithm Collaborative Computing with Photonic Spiking Neuron Chip Based on an Integrated Fabry–Perot Laser with a Saturable Absorber. *Optica* **2023**, *10*, 162–171. [CrossRef]
22. Xiang, S.; Shi, Y.; Zhang, Y.; Guo, X.; Zheng, L.; Han, Y.; Zhang, Y.; Song, Z.; Zheng, D.; Zhang, T.; et al. Photonic Integrated Neuro-Synaptic Core for Convolutional Spiking Neural Network. *Opto Electron. Adv.* **2023**, *6*, 230140. [CrossRef]
23. Romeira, B.; Javaloyes, J.; Ironside, C.N.; Figueiredo, J.M.L.; Balle, S.; Piro, O. Excitability and Optical Pulse Generation in Semiconductor Lasers Driven by Resonant Tunneling Diode Photo-Detectors. *Opt. Express* **2013**, *21*, 20931–20940. [CrossRef]
24. Yoo, S.; Kim, R.; Park, J.-H.; Nam, Y. Electro-Optical Neural Platform Integrated with Nanoplasmonic Inhibition Interface. *ACS Nano* **2016**, *10*, 4274–4281. [CrossRef]
25. Robertson, J.; Deng, T.; Javaloyes, J.; Hurtado, A. Controlled Inhibition of Spiking Dynamics in VCSELs for Neuromorphic Photonics: Theory and Experiments. *Opt. Lett.* **2017**, *42*, 1560–1563. [CrossRef]
26. Deng, T.; Robertson, J.; Wu, Z.-M.; Xia, G.-Q.; Lin, X.-D.; Tang, X.; Wang, Z.-J.; Hurtado, A. Stable Propagation of Inhibited Spiking Dynamics in Vertical-Cavity Surface-Emitting Lasers for Neuromorphic Photonic Networks. *IEEE Access* **2018**, *6*, 67951–67958. [CrossRef]
27. Nahmias, M.A.; Shastri, B.J.; Tait, A.N.; Prucnal, P.R. A Leaky Integrate-and-Fire Laser Neuron for Ultrafast Cognitive Computing. *IEEE J. Sel. Top. Quantum Electron.* **2013**, *19*, 1800212. [CrossRef]
28. Wang, Z.-J.; Xia, G.-Q.; Wu, Z.-M.; Tian, Z.-F.; Deng, T. Theoretical Investigation on the Propagation Characteristics of Inhibited Spiking Dynamics between Two VCSEL-Based Photonic Neurons. In Proceedings of the Semiconductor Lasers and Applications VIII, Beijing, China, 6 November 2018; Volume 10812, pp. 24–31.
29. Friart, G.; der Sande, G.V.; Khoder, M.; Erneux, T.; Verschaffelt, G. Stability of Steady and Periodic States through the Bifurcation Bridge Mechanism in Semiconductor Ring Lasers Subject to Optical Feedback. *Opt. Express* **2017**, *25*, 339–350. [CrossRef]
30. Mu, P.; He, P.; Li, N. Simultaneous Chaos Time-Delay Signature Cancellation and Bandwidth Enhancement in Cascade-Coupled Semiconductor Ring Lasers. *IEEE Access* **2019**, *7*, 11041–11048. [CrossRef]
31. Li, N.; Nguimdo, R.M.; Locquet, A.; Citrin, D.S. Enhancing Optical-Feedback-Induced Chaotic Dynamics in Semiconductor Ring Lasers via Optical Injection. *Nonlinear Dyn.* **2018**, *92*, 315–324. [CrossRef]
32. Wang, Y.; Wang, X.; Mu, P.; Guo, G.; Liu, X.; Wang, K.; He, P.; Hu, G.; Jin, G. Influence of Linewidth Enhancement Factor on the Nonlinear Dynamics and TDS Concealment of Semiconductor Ring Lasers. *Electronics* **2022**, *11*, 2007. [CrossRef]
33. Hurtado, A.; Javaloyes, J. Controllable Spiking Patterns in Long-Wavelength Vertical Cavity Surface Emitting Lasers for Neuromorphic Photonics Systems. *Appl. Phys. Lett.* **2015**, *107*, 241103. [CrossRef]
34. Li, B.; Memon, M.I.; Mezosi, G.; Yuan, G.; Wang, Z.; Sorel, M.; Yu, S. All-Optical Response of Semiconductor Ring Laser to Dual-Optical Injections. *IEEE Photonics Technol. Lett.* **2008**, *20*, 770–772. Available online: https://ieeexplore.ieee.org/abstract/document/4490023 (accessed on 1 July 2024). [CrossRef]
35. Beri, S.; Gelens, L.; Mestre, M.; Van der Sande, G.; Verschaffelt, G.; Scirè, A.; Mezosi, G.; Sorel, M.; Danckaert, J. Topological Insight into the Non-Arrhenius Mode Hopping of Semiconductor Ring Lasers. *Phys. Rev. Lett.* **2008**, *101*, 093903. [CrossRef]
36. Gelens, L.; Beri, S.; Van der Sande, G.; Mezosi, G.; Sorel, M.; Danckaert, J.; Verschaffelt, G. Exploring Multistability in Semiconductor Ring Lasers: Theory and Experiment. *Phys. Rev. Lett.* **2009**, *102*, 193904. [CrossRef]
37. Sorel, M.; Laybourn, P.J.R.; Scirè, A.; Balle, S.; Giuliani, G.; Miglierina, R.; Donati, S. Alternate Oscillations in Semiconductor Ring Lasers. *Opt. Lett.* **2002**, *27*, 1992–1994. [CrossRef]
38. Peng, H.-T.; Angelatos, G.; de Lima, T.F.; Nahmias, M.A.; Tait, A.N.; Abbaslou, S.; Shastri, B.J.; Prucnal, P.R. Temporal Information Processing with an Integrated Laser Neuron. *IEEE J. Sel. Top. Quantum Electron.* **2020**, *26*, 5100209. [CrossRef]